Virology 610 (2025) 110599

Contents lists available at ScienceDirect

Virology

journal homepage: www.elsevier.com/locate/virology

Synergistic effects of peptide mimics against enveloped viruses

Umme Laila Urmi [a,*], Ajay Kumar Vijay [a,c], Rajesh Kuppusamy [a,b,d], Samuel Attard [b], Lissy M. Hartmann [e], Samara Bridge [e], Suganeya Soundararajan [e], Stephen A. Holt [e,f], Sidra Sarwat [a], Salequl Islam [a,g], Charles G. Cranfield [e], Naresh Kumar [b], Mark D.P. Willcox [a,**]

[a] School of Optometry and Vision Science, University of New South Wales, Sydney, NSW, 2052, Australia
[b] School of Chemistry, University of New South Wales, Sydney, NSW, 2052, Australia
[c] University of Sydney, NSW, 2006, Australia
[d] Whiteley Corporation, Tomago, Newcastle, NSW, Australia
[e] School of Life Sciences, University of Technology Sydney, PO Box 123, Ultimo, 2007, Australia
[f] Australian Nuclear Science and Technology Organisation, Lucas Heights, NSW, 2234, Australia
[g] Department of Microbiology, Jahangirnagar University, Savar, Dhaka, 1342, Bangladesh

ARTICLE INFO

Keywords:
Antiviral peptide
Peptidomimetics
Synergy
Coronavirus
Influenza virus
Herpes simplex virus

ABSTRACT

The global health impact of viruses highlights the urgent need for innovative antiviral strategies. This study investigated the synergistic potential of two anthranilamide-based peptide mimics (RK610 and RK758) in combination, and one peptide mimic (RK610) in combination with the cationic peptides Mel4 and melimine, against murine hepatitis virus (a coronavirus; MHV-1), influenza virus (H1N1), and Herpes simplex virus (HSV-1). Checkerboard assays demonstrated RK610+RK758 had synergy against MHV-1 and H1N1 (∑FICI values of 0.14 and 0.5, respectively), while RK610+Mel4 showed potent synergy against HSV-1 (∑FICI = 0.18). Co-treatment outperformed sequential application. Transmission electron microscopy confirmed structural damage to virions, while cytotoxicity assays indicated that all tested combinations were non-toxic in MDCK, A9, and Vero cells, except for melimine and RK610+melimine with A9 cells. Biophysical analyses using DOPC (100 %) and DOPC: POPS (70:30) lipids provided mechanistic ideas into peptide-mimic interactions with lipid envelopes. Tethered bilayer lipid membranes (tBLMs) in conjunction with electrical impedance spectroscopy revealed that both peptide mimics and their combinations reduced membrane conductance, regardless of lipid composition. Quartz crystal microbalance with dissipation monitoring (QCM-D) revealed that RK610 and RK758 induced mass addition at the outer layer, significantly increasing with POPS. In DOPC, RK610 increased the surface pressure in a Langmuir-Blodgett trough while RK758 reduced it. The 610 + 758 and 610+Mel4 combinations raised maximum pressures. In DOPC + POPS, RK758 destabilized the monolayer (35 mN/m, no plateau), whereas combinations restored stability. These findings highlight peptide mimics as broad-spectrum antiviral agents that show synergy to target viral envelopes, paving the way for safer and low-resistance therapeutics.

1. Introduction

Viruses such as coronaviruses (e.g., SARS-CoV-2), influenza viruses, and Herpes simplex virus type 1 (HSV-1) represent significant global health challenges, causing widespread morbidity, mortality, and economic burden. Historical outbreaks like the 1918H1N1 influenza pandemic, which claimed an estimated 17.4 million deaths (Ó Gráda, 2024), and the ongoing COVID-19 pandemic, responsible for over 7.1 million deaths (Organization, 2024), demonstrate their devastating impact. Similarly, latent viral threats like HSV-1 (Bai et al., 2024) underscore the urgency for innovative antiviral solutions. Existing therapies often fall short during outbreaks, it takes time to develop vaccines,

* Corresponding author.
** Corresponding author.
E-mail addresses: m.urmi@unsw.edu.au (U.L. Urmi), v.ajaykumar@unsw.edu.au (A.K. Vijay), rajesh.kuppusamy@whiteley.com.au (R. Kuppusamy), s.attard@unsw.edu.au (S. Attard), Lissy.M.Hartmann@student.uts.edu.au (L.M. Hartmann), Samara.Bridge@student.uts.edu.au (S. Bridge), Suganeya.Soundararajan@student.uts.edu.au (S. Soundararajan), sph@ansto.gov.au (S.A. Holt), s.sarwat@unsw.edu.au (S. Sarwat), salequl@juniv.edu (S. Islam), Charles.Cranfield@uts.edu.au (C.G. Cranfield), n.kumar@unsw.edu.au (N. Kumar), m.willcox@unsw.edu.au (M.D.P. Willcox).

https://doi.org/10.1016/j.virol.2025.110599
Received 7 April 2025; Received in revised form 12 May 2025; Accepted 5 June 2025
Available online 6 June 2025

and viruses mutate to avoid their effects, which highlights the pressing need for novel approaches.

Antimicrobial peptides (AMPs) have emerged as promising therapeutic agents due to their broad-spectrum activity against viruses (Urmi et al., 2023, 2024) as well as bacteria (Dutta et al., 2017; Kruse et al., 2024; Rasul et al., 2010) and fungi (Souza, 2022). These molecules, whether naturally occurring or engineered, disrupt microbial membranes. However, challenges such as enzymatic degradation and high production costs limit their clinical utility. To overcome these issues, several synthetic analogues that can act against a variety of viruses including SARS-CoV-2 and other coronaviruses (Dahal et al., 2022; Urmi et al., 2023), influenza virus (Scala et al., 2023; Urmi et al., 2024), herpes simplex virus (HSV) (Liuzzi et al., 1994; Urmi et al., 2023), norovirus (Amblard et al., 2018), enterovirus (Dai et al., 2021), and human immunodeficiency virus (Neffe and Meyer, 2004), have been developed. These mimics retain the functional properties of AMPs while offering targeted activity and enhanced stability, as well as being cheaper to produce. Often, these mimics act by disrupting the lipid bilayers critical to the structural integrity of enveloped viruses (Kuppusamy et al., 2023; Urmi et al., 2023, 2024). While significant progress has been made in elucidating the features and functional mechanisms of peptide mimics, many critical aspects remain underexplored, presenting opportunities for further research.

Combination therapy involves the simultaneous use of multiple agents that may enhance efficacy, reduce resistance, and minimize side effects (Shyr et al., 2021). Synergistic or additive interactions between compounds increase therapeutic effectiveness while lowering required doses, thereby improving safety profiles. Synergy occurs when the combined effect of two agents exceeds the sum of their individual effects, while additive interactions produce outcomes equivalent to the sum of their separate effects. Both can allow drugs to achieve desired outcomes at lower doses, thereby minimizing toxicity and other side effects. Moreover, combination therapy may delay the emergence of drug resistance by targeting different microbial or cellular pathways simultaneously, making it particularly effective for rapidly mutating pathogens. Numerous studies have demonstrated the efficacy of combination therapies against a range of viruses, including Ebola virus (Sun et al., 2017), coxsackie B1 virus (Nikolaeva-Glomb and Galabov, 2004), enterovirus (Ianevski et al., 2022), influenza virus (Belardo et al., 2015), SARS-CoV-2 (Jeffreys et al., 2022), arenaviruses (Herring et al., 2021), cytomegalovirus (Chou et al., 2018), and HSV-1 and HSV-2 (Criscuolo et al., 2018). Although peptide-peptide combinations have been examined (Strandberg et al., 2015), the pairing of peptides with mimics or two mimics has received less attention.

Previously, peptide mimics RK610 and RK758 showed promising antiviral activity against enveloped viruses. Specifically, peptide RK610 had good efficacy against the coronavirus MHV-1, a surrogate for SARS-CoV-2, with an IC_{50} value of 2.38 μM, and against the influenza virus H1N1, with an IC_{50} value of 2.35 μM. Additionally, it showed moderate activity against Herpes simplex virus HSV-1, with an IC_{50} value of 34.9 μM (Urmi et al., 2023, 2024). In contrast, cationic peptides such as Mel4 and melimine were active against non-enveloped adenovirus and norovirus, mainly by disrupting the integrity of their capsids, but showed no efficacy against the enveloped influenza viruses (Urmi et al., 2023, 2024). Given the potent antiviral properties of peptide mimics, the aim of this study was to explore the mechanism of action of the combination of two mimics (RK610 and RK758) or pairing RK610 with AMPs (Mel4 or melimine) against enveloped viruses.

2. Material and methods

2.1. Peptides, mimics, and phospholipids

The peptides melimine and Mel4 were obtained from AusPep (Tullamarine, VIC, Australia), with both peptides having a purity of ≥90 %. The peptidomimetic compounds RK758 and RK610 used in this study were synthesized as described in patents WO2018081869A1 and Australian Provisional Patent Application No. 2021902457 (Kuppusamy et al., 2023; Urmi et al., 2024). 1,2-Dioleoyl-sn-glycero-3-phosphocholine bilayer (DOPC) and 1-palmitoyl-2-oleoyl-sn-glycero-3-phospho-L--serine (POPS) were purchased from Avantor Performance Materials (Poland S.A., Gliwice, Poland; purity >99.9 %).

2.2. Viruses and cells

The coronavirus mouse hepatitis virus type 1 (MHV-1) strain ATCC/VR261, and Herpes simplex virus type 1 (HSV-1) strain ATCC/VR-1493 were cultivated in A9 (ATCC CCL-1.4) and Vero (ATCC CCL-81) cell lines, respectively, using Dulbecco's Minimum Essential Medium (DMEM; Thermo Fisher Scientific, Waltham, MA, USA) enriched with 10 % fetal bovine serum (FBS) and 1 % antibiotics (streptomycin sulfate and penicillin G) and incubated at 37 °C, 5 % CO_2. Similarly, Madin-Darby Canine Kidney (MDCK; ATCC CRL-2936) cells were maintained in this medium and incubation conditions. The influenza virus H1N1 (A/PR/8/34; ATCC VR-1469) was propagated in MDCK cells with the addition of 2 μg/mL TPCK-treated trypsin (Thermo Fisher Scientific Australia Pty Ltd.) and 10 % bovine serum albumin (BSA 7.5 %; Bovogen Biologicals Pty Ltd., Melbourne, VIC, Australia). Virus stocks were then prepared and stored at −80 °C (Urmi et al., 2023, 2024).

2.3. Modified checkerboard assay for evaluating antiviral combinations

A modified checkerboard assay was used to study the combined antiviral effects of the peptide mimic RK610 (which had previously been shown to be active against influenza viruses (H1N1, H3N2), MHV-1 and HSV-1)(Urmi et al., 2023, 2024), with RK758, Mel4 or melimine against H1N1, MHV-1 and HSV-1. Each compound was tested starting at its IC_{50} concentration with two-fold serial dilutions prepared in plain DMEM along the rows (Compound A) and columns (Compound B) of a cell culture plate. The plate included wells with single compounds, combinations of compounds, and a control well containing no compounds. Viruses (2×10^3 PFU or $TCID_{50}$/ml) were added to each well and incubated for 3 h to allow interaction with the compounds. After incubation, the virus viability was measured using either a plaque assay for MHV-1 and HSV-1 or the $TCID_{50}$ method for H1N1. The percentage of inhibition was calculated by comparing the results with the control well. The wells approximating the IC_{50} values for combinations were identified to evaluate potential synergistic, additive, or antagonistic effects. Fractional inhibitory concentration indices (FICIs) were calculated to quantify the combination effect of compounds. The FICI was determined as the sum of FIC values for each compound (Fig. 1) (Luganini et al., 2011).

2.4. Time course study

To begin to study how peptide and mimic combinations work, a sequential time-course experiment was designed using a two-step incubation process. The combinations and concentrations were selected based on results from the checkerboard assay, which showed synergistic and additive interactions. For this study, the concentrations in combination that resulted in activity at one dilution below the most effective synergistic or additive concentrations were used to avoid overly strong effects that might hide smaller but important changes in how the compounds work. For the sequential addition experiment, compound RK610 was incubated with the virus for 1 h, and then the second compound was added, with both incubated together for an additional 2 h. For the co-treatment experiment, RK610 and the secondary compounds were added to the virus at the same time and incubated for 3 h. The viral reduction was measured using plaque assays for MHV-1 and HSV-1, and $TCID_{50}$ for H1N1. Control experiments, where the virus was incubated in plain DMEM without any compounds, were included for comparison. Results were expressed as the percentage of virus inhibition compared to

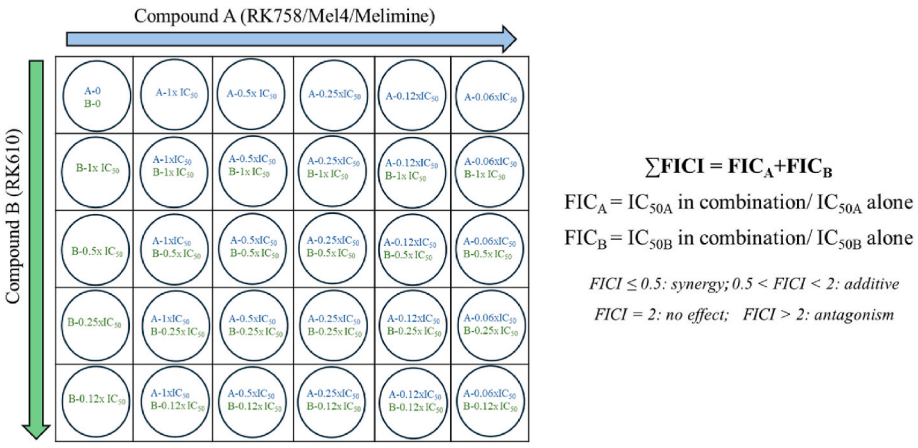

Fig. 1. Plate layout for checkerboard assays. The highest concentrations of each compound correspond to their respective IC_{50} values, with serial dilutions performed along the rows and columns to generate a gradient of combined concentrations. The fractional inhibitory concentration index (FICI) and the interpretations of ∑FICI values were calculated using the formula set out in the figure.

the control, allowing the effectiveness and interaction patterns of the sequential and co-treatment approaches to be analysed.

2.5. Transmission electron microscopy

Viruses were exposed to the synergistic concentration of the peptide and mimic combinations. For instance, MHV-1 was treated with RK610 (2.18 μM) + RK758 (23.7 μM), H1N1 with RK610 (2 μM) + RK758 (12.34 μM), and HSV-1 with RK610 (35 μM) + Mel4 (125 μM) (all in 1x phosphate buffer saline (PBS), pH 7.4) at 37 °C for 2 h. Following treatment, 10 μL aliquot of the virus mixture was applied to a glow-discharged, carbon-coated copper grid (200 mesh) and allowed to adsorb for 5 min at room temperature to facilitate maximum attachment of the virus particles to the grid. Excess fluid was then gently removed using filter paper, and the grid was carefully washed three times in large drops of distilled water to remove any unbound particles. Immediately following the final wash and removal of excess water with filter paper, the sample was stained with 2 % w/v phosphotungstic acid (PTA, pH 4.5) for 30 s to enhance image contrast. After drying, grids were analysed using a transmission electron microscope (TEM; FEI Tecnai G2 20, Hillsboro, Oregon, USA). Control samples were prepared in 1x PBS only. Images were observed to identify appearance differences between the treatment and control groups (Urmi et al., 2023, 2024).

2.6. Cytotoxicity

To assess the cytotoxic effects of peptide and mimic combinations on MDCK, A9, and Vero cells, a 3-(4,5-dimethylthiazol-2-yl)-2,5-diphenyltetrazolium bromide (MTT) assay was performed. Each combination of concentrations that showed synergistic or additive effects with their viruses and the respective cell lines was tested both as a mixture and as individual components to evaluate any changes in cytotoxicity when used together versus separately (Table 2). Cells were seeded in 96-well plates at a density of 5000 cells per well and cultured at 37 °C in a humidified atmosphere containing 5 % CO_2 for 24 h. They were then treated with the test combinations and concentrations for 24 h. After treatment, 100 μL of 5 mg/mL MTT solution was added to each well and incubated at 37 °C for 2–4 h. Following incubation, the supernatant was discarded, and 100 μL of 100 % DMSO was added, with 10 min of vigorous shaking at room temperature to dissolve the formazan crystals. Absorbance was measured at 540 nm using a spectrophotometer to determine cytotoxicity, calculated by comparing absorbance in treated wells to control wells and expressed as a percentage. Positive controls for cell death used 100 μL DMSO, while negative controls used 100 μL of culture medium (Urmi et al., 2023, 2024).

2.7. Assessment of compound interactions

^{1}H Nuclear Magnetic Resonance (NMR) spectroscopy was used to determine whether the compounds could interact together, in the absence of a membrane-mimetic environment. Samples were prepared by dissolving RK610, RK758, RK610+RK758, and RK610+Mel4 in equimolar concentrations. Each compound or combination was dissolved in DMSO-d6, a deuterated solvent suitable for NMR analysis. The experiments were conducted using a Bruker Advance III 400 MHz NMR spectrometer, which provides high-resolution spectra for detailed structural and interaction analysis. After data acquisition, the NMR spectra were processed and analysed using MestreNova software, enabling precise interpretation of chemical shifts, peak integration, and other spectral features. This method ensured accurate characterization of the peptide mimics and their potential interactions in a non-biological environment (Aldilla et al., 2022).

2.8. Tethered bilayer lipid membranes (tBLMs)

To explore interactions between lipids with the peptides or mimics, two distinct lipid bilayer compositions (100 % DOPC or 70:30 ratio of DOPC/POPS) were tested using the tethered bilayer lipid membrane (tBLM) technique (Hartmann et al., 2022). The lipid bilayers were assembled on gold slides coated with 10 % tethered benzyl-disulfide tetraethyleneglycol phytanyl "tethers" and 90 % benzyl-disulfide-tetra-ethyleneglycol-OH "spacer" molecules (SDx Tethered Membranes Pty Ltd., Roseville, NSW, Australia). Onto these slides, 8 μL of a 3 mM solution of mobile lipid was applied. After a brief 2-min incubation, the lipid films were thoroughly rinsed with 100 mM NaCl in 10 mM tris buffer, pH 7. The compounds were prepared in a similar buffer solution of 100 mM NaCl and 10 mM tris at pH 7, then applied to the tBLMs in gradually increasing concentrations, from 0.1 μM to 50 μM. To examine the influence of peptide and mimics on these membranes, AC electrical impedance spectroscopy (EIS) was used to track time-dependent shifts in membrane conductance (Gm) and capacitance (*Cm*). These measurements were performed using a tethaPod device (SDx Tethered Membranes). The data were modelled using an equivalent circuit that included a constant phase element, representing the imperfect capacitance of the tethering gold electrode, which was connected in series with a resistor-capacitor network representing the lipid bilayer, and a resistor to account for the impedance of the surrounding electrolyte solution, as previously described (Berry et al., 2018). To ensure precise analysis, Gm and *Cm* values were normalized against initial baseline conductance and capacitance readings taken before the addition of any compounds, allowing for control over

baseline variation among different tBLM samples (Bahatheg et al., 2024; Berry et al., 2018).

2.9. Quartz crystal microbalance with dissipation (QCM-D)

Quartz crystal microbalance with dissipation monitoring (QCM-D) was conducted using the QSense analyzer system (Biolin Scientific, Stockholm, Sweden) with solid-supported lipid bilayers (SLBs) on a silica surface. This technique depends on the piezoelectric properties of a quartz sensor crystal to detect relative changes in mass on its surface by measuring shifts in frequency (ΔF) and energy dissipation (ΔD). The two types of lipid composition used in this study were: 100 % DOPC and a 70:30 mol% mixture of DOPC/POPS. The technique investigated the interactions of RK758 (10 μM), RK610 (10 μM), Mel4 (10 μM), RK610 (5 μM) + RK758 (5 μM), and RK610 (5 μM) + Mel4 (10 μM) with these SLBs. A baseline was first established using tris-buffered saline (100 mM NaCl, 10 mM Tris, pH 7.0) pumped at 300 μL/min for 4 min to stabilize the system. Following that, lipid vesicles (150 μM) were introduced at a flow rate of 50 μL/min for 10 min. The system was subsequently rinsed with tris-buffered saline (300 μL/min) for 5 min, deionized water (300 μL/min) for 5 min, and again with tris-buffered saline (300 μL/min) for 5 min to ensure the formation of a stable bilayer (McCubbin et al., 2011).

To evaluate peptide and mimic interactions, solutions containing the compounds in tris-buffered saline were flowed over the SLBs at 50 μL/min for 10 min, followed by a 10-min incubation period without flow. A final rinse with tris-buffered saline was performed until the frequency and dissipation values stabilized. The ΔF and ΔD values reported throughout this study represent the differences between the stable bilayer baseline (just before peptide or mimic injections) and the stabilized values after the final rinse. Overall data for each experiment are presented as ΔF-ΔD plot, and ΔF and ΔD values were recorded at the 3rd, 5th, 7th, 9th, and 11th harmonics (overtones) of the QCM-D crystal's resonant frequency. Due to the varying penetration depths of acoustic waves at different harmonics, higher overtones (e.g., 9th and 11th) are associated with processes closer to the crystal surface, while lower overtones reflect activity near the outer surface of the mass (John et al., 2018). Consistent ΔF and ΔD values across all overtones suggested that the observed effects occurred uniformly throughout the thickness of the bilayer (John et al., 2018; McCubbin et al., 2011; Mechler et al., 2007; Wang et al., 2015).

2.10. Langmuir-Blodgett (LB) test for lipid monolayer interaction

A Langmuir trough was used to evaluate the interaction of compounds (RK610, RK758, RK610+RK758, and RK610+Mel4) with lipid monolayers (Kim et al., 2020; Perez-Lopez et al., 2009; R Dennison et al., 2010). DOPC and POPS were dissolved in chloroform at a concentration of 1 mg/mL. The experiments were conducted using Langmuir–Blodgett (KSV, 2000 Standard, KSV Instruments, Helsinki, Finland) and Langmuir (KSV Nima, Biolin Scientific, Stockholm, Sweden) troughs, both equipped with symmetric barriers and a Wilhelmy plate for surface tension determination. Surface pressure–area isotherms were obtained using these setups. Lipid monolayers were prepared with two compositions: 100 % DOPC and a mixture of 70 % DOPC+30 % POPS. A 100 μL aliquot of the 1 mg/mL lipid solution (dissolved in chloroform) was delivered using a Hamilton syringe, which was spread onto the subphase surface. The subphase consisted of the tris-buffered saline. After spreading, the chloroform was allowed to evaporate for 15 min to ensure the formation of a stable monolayer. The monolayer was then compressed symmetrically over the surface area of 15–75 cm^2 at a constant rate of 10 mm/min to obtain surface pressure–area isotherms. For compound interaction studies, the compounds were carefully added by direct application on top of the monolayer, achieving a final bulk-phase concentration of 1.5 μM. The surface pressure was measured for both lipid-only monolayers and those containing the added compounds. The change in surface pressure was quantified by comparing the initial surface pressure of the lipid monolayer to the surface pressure recorded after compound addition.

2.11. Statistics

All experiments were performed in triplicate, and the results are presented as the mean ± standard error of the mean (SEM). Statistical analysis was performed using GraphPad Prism (version 9.5.0). A one-way ANOVA was applied, followed by a non-parametric Kruskal-Wallis test with Dunn's multiple comparisons, using a 95 % confidence level. A p-value of less than 0.05 was considered statistically significant, with significance levels indicated as follows: *$p < 0.05$, **$p < 0.01$, ***$p < 0.001$, ****$p < 0.0001$. Results labelled as "ns" showed no statistically significant differences.

3. Results

3.1. Antiviral activity of peptide and mimic combinations

Individually, the mimic RK610 exhibited strong antiviral effects against MHV-1 (IC_{50} = 2.18 μM) and H1N1 (IC_{50} = 2 μM) but showed only moderate activity against HSV-1 (IC_{50} = 35 μM). The mimic RK758 demonstrated moderate antiviral activity against MHV-1, H1N1, and HSV-1 with IC_{50} values of 23.7 μM, 12.34 μM, and 25 μM, respectively. Peptides Mel4 and Melimine, however, showed no measurable activity against any of the tested enveloped viruses (Urmi et al., 2023, 2024). The current combination study aimed to understand the combined effect of peptide mimics RK610 and RK758 and whether mimic RK610 could enhance the activity of the AMPs Mel4 and melimine. The checkerboard assay represented in Fig. 1 and the heatmap presented in Fig. 2, along with the results summarized in Table 1, collectively demonstrate the combined effects of these compounds.

Against H1N1, the combination of mimics RK610 and RK758 resulted in a reduced combined IC_{50} (RK610 = 0.5 μM; RK758 = 3.1 μM) compared to their individual IC_{50} values (RK610 = 2 μM; RK758 = 12.34 μM), with an ∑FICI of 0.5, indicating synergy. The combinations of RK610 with Mel4 or Melimine exhibited ∑FICI values of 1 and 0.75, respectively, reflecting additive effects. For MHV-1, the combination of RK610 and RK758 demonstrated strong synergy, with an ∑FICI of 0.14, while the combinations of RK610 with Mel4 or Melimine showed additive effects (∑FICI values of 0.73 and 1, respectively).

In the case of HSV-1, the combination of RK610 and RK758 exhibited an additive effect (∑FICI = 0.75), whereas the combination of RK610 and Mel4 demonstrated strong synergy, with a ∑FICI of 0.18. Interestingly, the combination of RK610 and melimine showed no interaction against HSV-1 (∑FICI = 2). Overall, these results underscore the potential of combinations to achieve enhanced antiviral activity at lower concentrations. Notably, no antagonistic interactions (∑FICI >2) were observed in any of the tested combinations, indicating that the compounds complement each other without compromising effectiveness.

3.2. Comparison of sequential and co-treatment of peptide and mimic combinations

Co-treatment, both compounds incubated together with viruses for 3 h, consistently exhibited better antiviral activity (Fig. 3) compared to sequential treatment (RK610 incubated with viruses for 1 h, followed by addition of second compound and incubation for 2 h) for all tested peptide and mimic combinations.

3.3. TEM imaging

To evaluate the synergistic effects of these compound combinations on viral integrity, specific concentrations were tested for each virus. For H1N1 (Fig. 4A) (Supplementary Fig. 1A), control virions appeared intact, characterized by smooth, spherical particles with well-defined

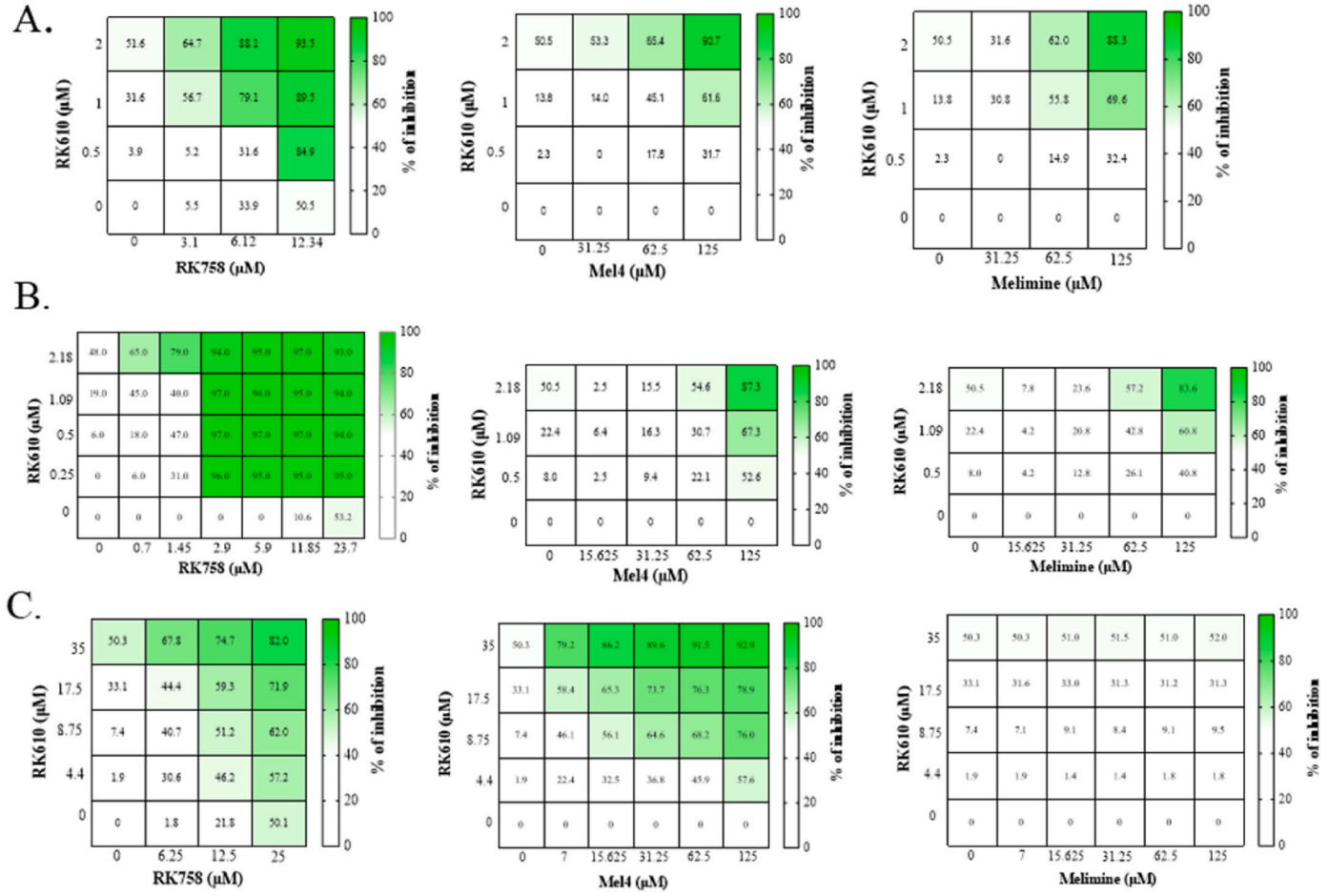

Fig. 2. Heatmap representation of checkerboard assays of peptides and mimics against the enveloped viruses (A) H1N1, (B) MHV-1, and (C) HSV-1. The rows represented the concentrations of RK758, Mel4, and melimine, while the columns represented the concentrations of RK610. Each heatmap demonstrated the percentage of inhibition of viruses for individual compounds and their combinations compared to the control. Data shown were from three representative biological replicates. Green shading indicates percentage of viral inhibition, with darker shading indicating higher viral inhibition and lighter shading or white areas represent minimal or no inhibition. (For interpretation of the references to colour in this figure legend, the reader is referred to the Web version of this article.)

Table 1
Combination of effect of peptides and mimics against viruses.

Virus	Peptide/Mimics		Peptide/Mimics		∑FICI[a]	Effect
	Individual IC_{50} (μM)		Combined IC_{50} (μM)			
Compounds	**RK610**	**RK758**	**RK610**	**RK758**		
H1N1	2	12.34	0.5	3.1	0.5	Synergy
MHV-1	2.18	23.7	0.25	0.7	0.14	Synergy
HSV-1	35	25	8.75	12.5	0.75	Additive
Compounds	**RK610**	**Mel4**	**RK610**	**Mel4**		
H1N1	2	>125	1	62.5	1	Additive
MHV-1	2.18	>125	0.5	62.5	0.73	Additive
HSV-1	35	>125	4.4	7	0.18	Synergy
Compounds	**RK610**	**Melimine**	**RK610**	**Melimine**		
H1N1	2	>125	1	31.25	0.75	Additive
MHV-1	2.18	>125	1.09	62.5	1	Additive
HSV-1	35	>125	35	>125	2	No interaction

[a] ∑FICI = Summation of fractional inhibitory concentration index.

outer membranes and visible spikes. However, treated virions showed significant structural disruptions, with aggregated and fragmented particles, loss of membrane integrity, and deformation (Fig. 4A) (Supplementary Fig. 1A). Similarly, for MHV-1 (Fig. 4B) (Supplementary Fig. 1B), the control virions were intact, spherical structures with well-defined envelopes and surface spikes. In contrast, treated virions had substantial morphological disruptions, including deformed envelopes and fragmented or collapsed cores, suggesting that the treatment compromised viral integrity (Fig. 4B) (Supplementary Fig. 1B). These observations suggested that the combination of RK610 and RK758 destabilized the viral envelope, which may have contributed to the loss of infectivity. For HSV-1 (Fig. 4C) (Supplementary Fig. 1C), control virions retained a dense core and a well-defined outer envelope. In contrast, the treated virions appeared less dense, with a compromised

Table 2
Concentrations of peptide and mimic combinations tested on MDCK, A9, and Vero cells, and corresponding average percentage of cell viability.

Cells	Compounds and Concentrations tested	Percentage of cell viability (average %)
A9	RK610 (0.25 μM)	96.6
	RK758 (0.7 μM)	97.8
	RK610 (0.25 μM) + RK758 (0.7 μM)	100
	RK610 (0.5 μM)	85.8
	Mel4 (62.5 μM)	88.0
	RK610 (0.5 μM) + RKMel4 (62.5 μM)	93.5
	RK610 (1.09 μM)	86.4
	Melimine (62.5 μM)	6.4
	RK610 (1.09 μM) + melimine (62.5 μM)	5.9
MDCK	RK610 (0.5 μM)	88.4
	RK758 (3.1 μM)	88.4
	RK610 (0.5 μM) + RK 758 (3.1 μM)	92.1
	RK610 (1 μM)	87.5
	Mel4 (62.5 μM)	78.6
	RK610 (1 μM) + Mel4 (62.5 μM)	84.9
	RK610 (1 μM)	87.5
	Melimine (31.25 μM)	96.9
	RK610 (1 μM) + melimine (31.25 μM)	100
Vero	RK610 (8.75 μM)	90
	RK758 (12.5 μM)	100
	RK610 (8.75 μM) + RK758 (12.5 μM)	100
	RK610 (4.4 μM)	93.5
	Mel4 (7 μM)	86.4
	RK610 (4.4 μM) + Mel4 (7 μM)	87.4

envelope and a faint or diffused core (Fig. 4C) (Supplementary Fig. 1C). Overall, these findings highlighted the antiviral potential of these compound combinations, with their mechanism of action centred on destabilizing viral envelopes and impairing structural integrity across multiple viral models.

3.4. Cytotoxicity

After evaluating the combination effects of RK758, Mel4, and melimine with peptide mimic RK610 against viruses, their additive and synergistic concentrations were further tested for cytotoxicity on the respective cell lines: MDCK (H1N1), A9 (MHV-1), and Vero (HSV-1). The combined IC_{50} concentrations of peptides and mimics (Table 2) were tested both individually and in combination (Table 2). For MDCK cells, the tested combinations exhibited low cytotoxicity, with all conditions, whether tested alone or in combination, showing ≥70 % cell viability. In A9 cells, the combination of RK610 with RK758 or Mel4 displayed no cytotoxic effects either alone or in combination. However, the combination of RK610 with melimine or melimine alone was cytotoxic to A9 cells. Lastly, for Vero cells, the combinations of RK610 with RK758 and RK610 with Mel4 did not show any cytotoxic effects (≥85 % viability; Table 2).

3.5. Peptide synergy depends on biological surfaces: NMR studies

NMR analysis (Supplementary Fig. 2) of RK610, RK758, Mel4, and their combinations (RK610+RK758 and RK610+Mel4) revealed no direct interactions in non-biological environments, as no peak shifts were observed in the ^{1}H NMR spectra. This suggested that peptide interactions and their synergistic effects are primarily mediated by biological surfaces.

3.6. Evaluation of the individual and combined effects of peptide mimics on lipid membranes

The interactive and synergistic effects of peptide and mimic combinations were investigated further using tBLM, QCM-D, and LB techniques against two distinct lipid compositions: a membrane composed entirely of 100 % DOPC and another consisting of a 70:30 mol% mixture of DOPC and POPS. In tBLM studies, the individual compounds RK610 (10 μM) and RK758 (10 μM) showed minimal impact on the conductance of both lipid bilayers (DOPC and DOPC + POPS), indicating limited interaction with the membrane. Mel4 did not exhibit any measurable attachment to either lipid bilayer, suggesting a lack of interaction under the experimental conditions (Supplementary Fig. 3A). The combinations of RK610 (5 μM) + RK758 (5 μM) and RK610 (5 μM) + Mel4 (10 μM) induced a significant reduction in bilayer conductance, indicating stronger interactions with the lipid membranes. For DOPC membranes, the RK610+RK758 combination demonstrated a more pronounced decrease in conductance compared to RK610+Mel4, highlighting a greater synergistic effect when RK610 and RK758 were combined (Fig. 5). A similar trend was observed in the presence of serine-containing lipid layers (DOPC + POPS), where the combinations again showed a significant reduction in conductance compared to the individual compounds, further supporting the synergistic effects of the combinations (Fig. 5). During the washing step, the effects of the combinations on DOPC membranes remained unchanged, whereas the final reductions in conductance were diminished a bit in the DOPC + POPS membranes after washing (Fig. 5). Overall, a reduction in conductance suggested that the peptide mimics or their combinations were interacting with the lipid bilayers in a way that alters their electrical properties. In contrast to conductance, no significant changes were observed in capacitance for either the individual compounds or their combinations (Fig. 5).

To further investigate these effects, QCM-D experiments were conducted. Data were recorded until the frequency (ΔF) and dissipation (ΔD) values stabilized, marking the completion of the experiment. For compound RK610 interacting with the DOPC lipid layer, a frequency shift of −4.8 Hz was observed at the 3rd overtone, indicating higher mass adsorption at the outer layer. This was accompanied by a slight decrease in rigidity (viscoelasticity) at the outer layer compared to the inner layer. Notably, the changes in mass and rigidity were not reversible upon washing, suggesting strong and irreversible interactions between RK610 and the lipid membrane. The ΔF *vs.* ΔD plot for RK610 against DOPC revealed (Fig. 6A) a linear relationship, indicating that the impact on mass (weight) and rigidity was proportional. In the presence of POPS (DOPC + POPS), compound RK610 showed even greater mass adsorption at the outer layer, with a frequency shift of −14.5 Hz (3rd overtone), significantly higher ($p < 0.0001$) than that observed for 100 % DOPC. This was accompanied by a decrease in rigidity across the bilayer. The mass change was somewhat reversible upon washing, whereas the rigidity change was largely irreversible. The ΔF *vs.* ΔD plot in this case displayed a non-linear relationship, suggesting that the impact on mass and rigidity was not proportional. For both lipid layers, the outer layer (overtones 3rd and 5th) experienced a more pronounced effect than the inner layer (overtones 7th, 9th, and 11th), further emphasizing the compound's preferential interaction with the outer membrane surface (Fig. 6A).

The other mimic, RK758, exhibited a similar interaction pattern to RK610 with both lipid membranes. For the DOPC membrane, RK758 induced a frequency shift of −6.5 Hz at the 3rd overtone, indicating mass adsorption at the outer layer. In the presence of POPS, the mass adsorption was even greater, with a maximum frequency shift of −12 Hz. For both membranes, a decrease in rigidity was observed. For the DOPC membrane, this was a much more significant effect at the outer layer compared to the inner layer. For DOPC + POPS, the change in rigidity was consistent across the membrane. The primary difference between the two systems was observed during the washing step. For the

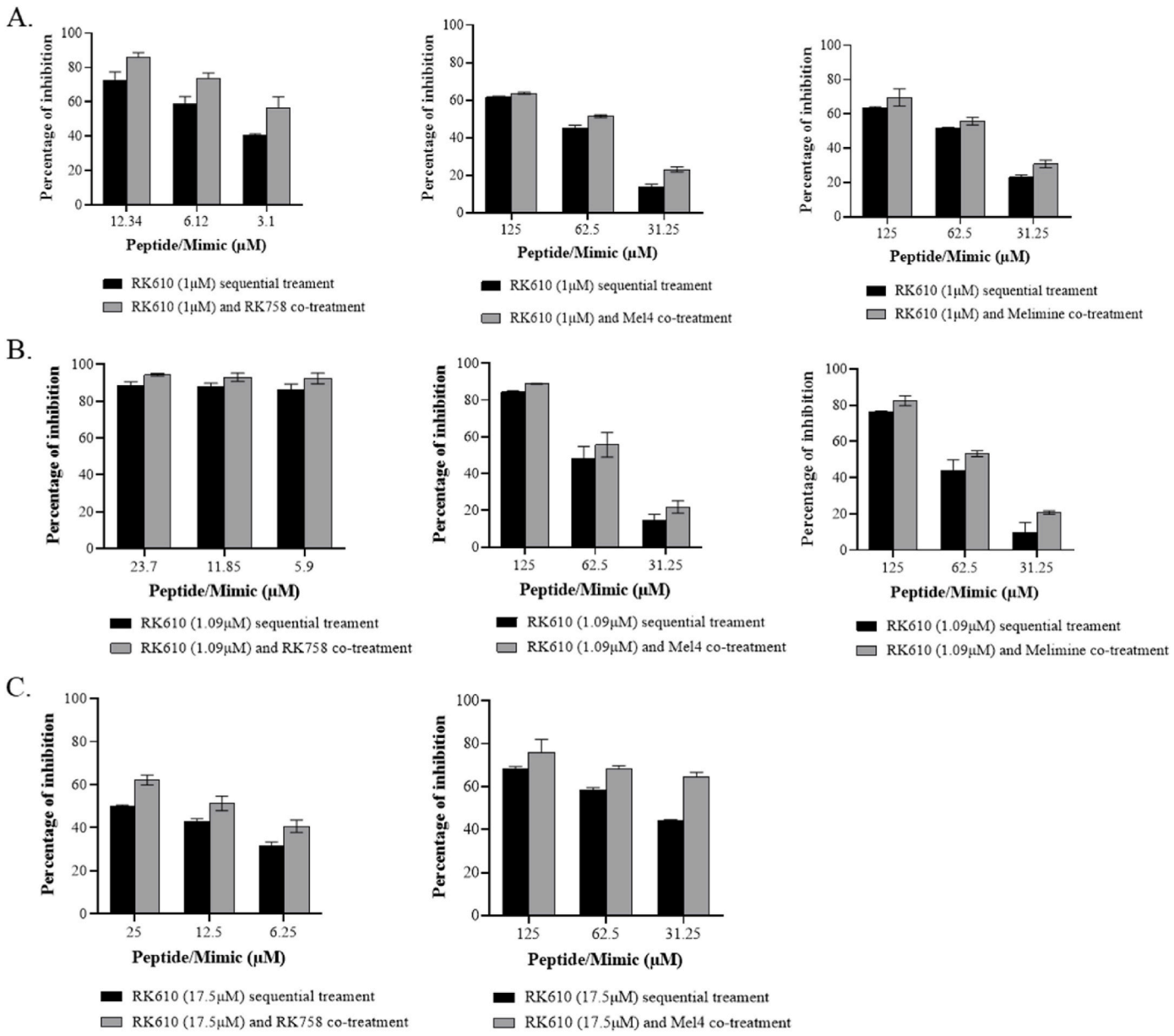

Fig. 3. Antiviral efficacy of sequential and co-treatment of peptide and mimic combinations against (A) H1N1, (B) MHV-1, and (C) HSV-1. The antiviral effects of sequential and co-treatment strategies were evaluated for combinations of peptide mimic RK610 with RK758, Mel4, or melimine. In sequential treatment, RK610 was pre-incubated with the viruses for 1 h, followed by the addition of the secondary compound for 2 h. In co-treatment, the viruses were exposed to both compounds simultaneously for 3 h. Virus viability was quantified and compared between the two approaches. Data are presented as mean ± SEM from three independent experiments.

DOPC membrane, the changes in mass and rigidity were not reversible upon washing, suggesting strong and irreversible interactions. In contrast, for the POPS-containing membrane, the mass change was somewhat reversible upon washing, while the rigidity change remained largely irreversible. The ΔF *vs.* ΔD plots further highlighted the differences between the two systems. For the DOPC membrane, the linear relationship indicated that the impact on mass and rigidity was proportional, with a more pronounced effect on the outer layer compared to the inner layer. In contrast, for the POPS-containing membrane, the non-linear relationship suggested that the impact on mass and rigidity was not proportional, suggesting a different mechanism of action, though the outer layer still experienced a greater effect than the inner layer (Fig. 6B). Overall, both peptide mimics, RK610 and RK758, demonstrated similar interaction patterns with lipid membranes, with key differences arising primarily in the reversibility of mass changes and the proportionality of mass-to-rigidity effects (Fig. 6).

For the RK610+RK758 combination interacting with the DOPC lipid layer, significant mass adsorption was observed at the outer layer, with a frequency shift of −7.5 Hz. The ΔF *vs.* ΔD plot revealed a non-linear relationship, suggesting that the impact on mass and rigidity was not proportional. In the case of the POPS-containing lipid membrane, the combination exhibited even greater mass adsorption, with a frequency shift of −25.5 Hz and the ΔF *vs.* ΔD plot displayed a linear relationship, indicating that the impact on mass and rigidity was proportional. For both lipid membranes, the RK610+RK758 combination caused a decrease in rigidity at the outer layer compared to the inner layer, along with greater mass adsorption at the outer layer with both effects being much more pronounced on POPS-containing membranes. Additionally, the membranes displayed differences in the reversibility of mass change, which was much more pronounced on DOPC membranes compared to

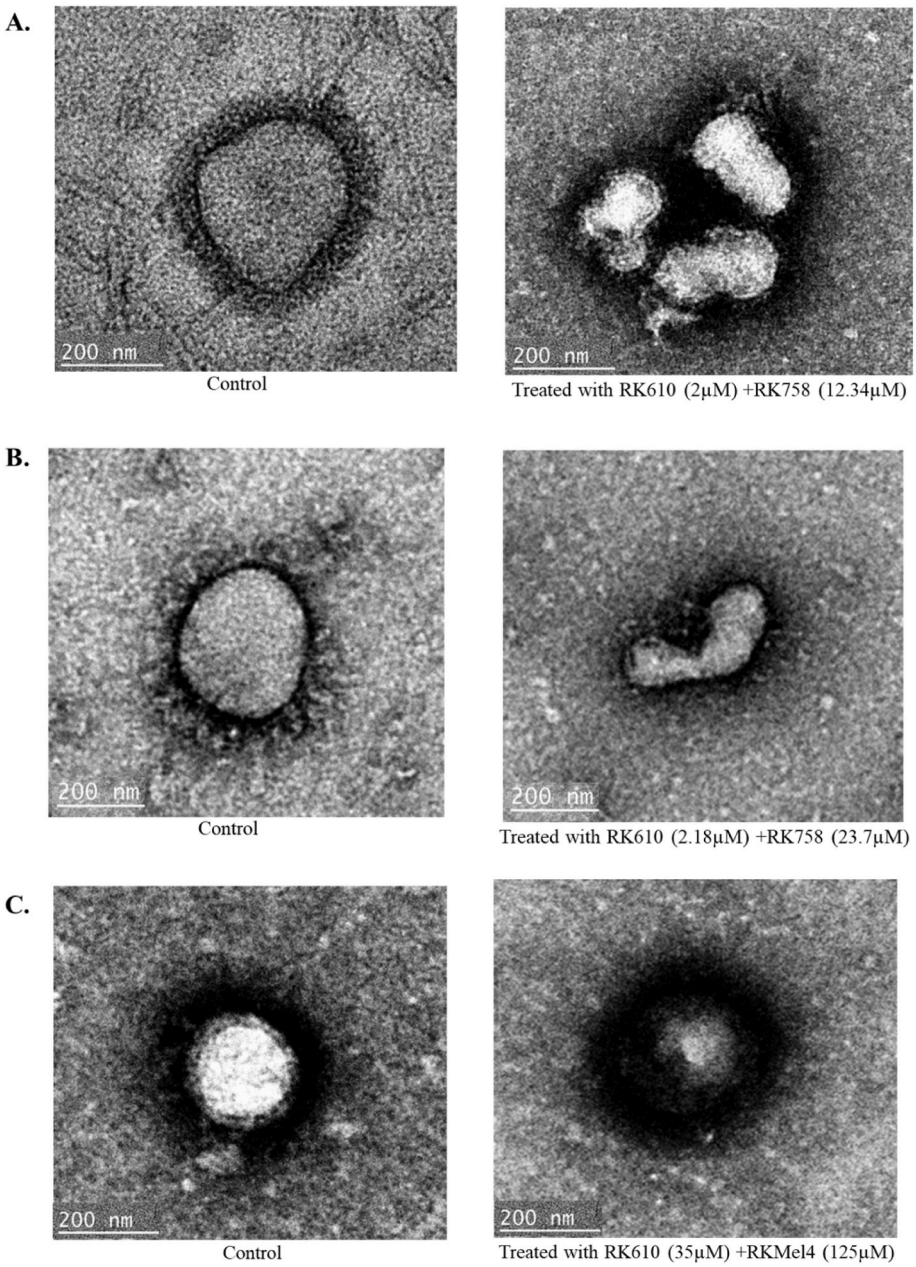

Fig. 4. Transmission electron microscopy (TEM) images of viruses after treatment with combination of compounds. A. H1N1: The left panel displays a structurally intact H1N1 virion, characterized by a well-defined envelope and core. In contrast, following treatment with RK610 (2 μM) + RK758 (12.34 μM), the right panel reveals significant morphological alterations, including disrupted structures and aggregated virions. **B**. MHV-1: The left panel showed an intact MHV-1 particle with a preserved envelope and well-maintained structural integrity. The right panel, however, demonstrates a collapsed core and disrupted envelope, indicative of extensive structural destabilization induced by the combination treatment with RK610 (2.18 μM) + RK758 (23.7 μM). **C**. HSV-1: The left panel shows an intact HSV-1 virion, with a dense core and a clear, defined envelope. The right panel illustrates changes following exposure to RK610 (35 μM) + Mel4 (125 μM), with notable structural compromise, including disorganization of the core and loss of envelope integrity.

POPS-containing membranes, while the rigidity reversed more on POPS-containing membranes (Fig. 7A).

In contrast, Mel4 alone did not exhibit detectable changes in frequency (ΔF) or dissipation (ΔD) (Supplementary Fig. 3B), suggesting a lack of interaction with the lipid bilayer. However, the RK610+Mel4 combination showed a distinct behaviour. For DOPC membranes, weight addition was observed across all layers, accompanied by a stronger decrease in rigidity at the outer layer compared to the inner layer. Notably, the changes in weight and rigidity were not reversible upon washing, indicating strong interactions with the DOPC membrane. Although the signals were minimal, the observed weight addition and rigidity changes could suggest partial insertion of the compounds across the membrane. The ΔF *vs.* ΔD plot revealed minimal changes, making it difficult to understand a clear direction, though there was a slightly more pronounced change in rigidity at the outer layer. For both DOPC and POPS-containing membranes, the RK610+Mel4 combination exhibited weight addition across all layers and a negligible decrease in rigidity. However, washing of POPS-containing membranes led to an increase in weight, possibly due to the membrane absorbing buffer components, while a slight decrease in rigidity was observed across all layers. The ΔF *vs.* ΔD plot indicated an initial removal of weight upon compound addition, followed by a subsequent increase in weight, suggesting a complex interaction mechanism (Fig. 7B).

Surface pressure data, obtained using the Langmuir-Blodgett trough,

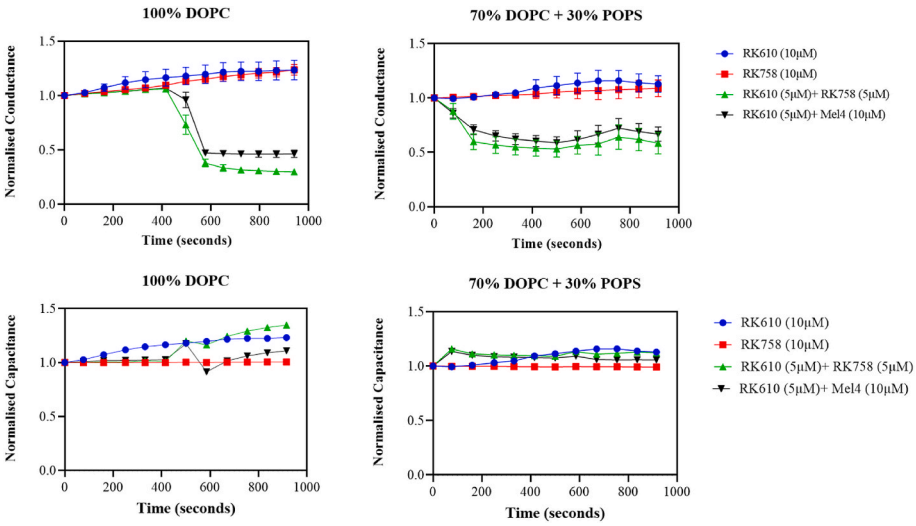

Fig. 5. The effect of peptide mimics and their combinations on the conductance and capacitance of DOPC and DOPC + POPS tethered bilayer lipid membranes (tBLMs).

revealed distinct behaviours for DOPC and DOPC + POPS lipid monolayers treated with individual compounds and their combinations. For the DOPC monolayer (Fig. 8A), the control curve exhibited a maximum pressure of 42 mN/m, indicating the highest surface pressure at which the monolayer remained stable under compression (plateau area), reflecting dense lipid packing. When RK610 was added, the maximum pressure increased slightly to 44 mN/m ($p > 0.9$), while the plateau area decreased marginally. In contrast, the addition of RK758 reduced the maximum pressure significantly to 36 mN/m ($p < 0.0001$), with a visible decrease in the plateau area. For the RK610+RK758 combination, the maximum pressure increased to 44 mN/m ($p = 0.17$), but the plateau area decreased. Similarly, the RK610+Mel4 combination showed an increased maximum pressure of 45 mN/m ($p > 0.9$), with a slight reduction in the plateau area.

For the DOPC + POPS monolayer (Fig. 8B), the control curve exhibited a maximum pressure of 38 mN/m. The addition of RK610 did not significantly ($p > 0.9$) alter the maximum pressure, but the plateau area increased. In contrast, RK758 ($p = 0.002$) reduced the maximum pressure to 35 mN/m, and no plateau area was detected, suggesting a loss of monolayer stability. The RK610+RK758 combination increased the surface pressure to 39 mN/m ($p = 0.9$), with a slight increase in the plateau area. Lastly, the RK610+Mel4 combination decreased the pressure to 36 mN/m ($p = 0.7$), with no significant change in the plateau area.

4. Discussion

This study provided a comprehensive assessment of the activities of peptide mimics, focusing on their synergistic potential and lipid membrane interaction mechanisms. The findings highlighted the potential of harnessing synergistic and additive interactions between peptides and mimics to enhance antiviral efficacy while maintaining non-cytotoxic effects. Mimic RK610 has potent antiviral activity against MHV-1 and H1N1, with IC_{50} values significantly lower than those observed for HSV-1 (Urmi et al., 2023, 2024). Mimic RK758, though less potent, displayed moderate activity across all tested viruses. When combined, RK610 and RK758 exhibited strong synergy against MHV-1 and H1N1, evidenced by reduced IC_{50} values and low $\sum$FICI values. These results suggested complementary mechanisms of action that amplify the antiviral effects of these peptide mimics. For HSV-1, a notable synergy was observed between RK610 and Mel4, with Mel4 inactive on its own. In contrast, the combination of RK610 and melimine against HSV-1 showed no interaction. Importantly, no antagonistic effects were detected for any combinations, confirming compatibility and cooperative action. Simultaneous co-treatment consistently outperformed sequential treatment, indicating that co-treatment allows peptide mimics to interact more effectively with viral particles, enhancing the disruption of viral integrity. TEM imaging provided further evidence of the structural damage to virions. For MHV-1 and H1N1, combination treatments resulted in severe envelope disruption and capsid fragmentation, consistent with impaired infectivity, while previous studies suggested that peptide mimics when used alone targeted the envelope but left the capsid intact (Urmi et al., 2023, 2024). For HSV-1, the combination of RK610 and Mel4 caused both envelope damage and core destabilization, a synergistic effect not seen with a single peptide mimic (Urmi et al., 2023). Besides these, cytotoxicity assays confirmed the safety of the tested combinations in MDCK, A9, and Vero cells, except for melimine-containing combinations, which exhibited inherent cytotoxicity. These findings highlighted the importance of selecting non-toxic combinations for therapeutic applications.

While no direct interaction between the peptide mimics or combinations was observed in non-biological environments via NMR, the observed enhancement in antiviral activity and membrane disruption in biological settings suggests a membrane-dependent or environment-mediated synergy. The mechanism behind this synergy is not yet fully understood but could involve cooperative membrane insertion, sequential membrane destabilization, or localized concentration effects that increase activity when both agents are present (Drajkowska and Molski, 2025). Further investigation into the exact nature of the interactions, whether electrostatic, hydrophobic, or otherwise, will be necessary to clarify the mechanism. A similar phenomenon had been reported between the peptides LL-37 and HNP-1, where they did not interact under physical conditions but complemented each other in biological environments (Grassin). Overall, there had been very few studies investigating the combination effect of two peptide mimics or peptide and mimics. Previously, RK758 mimic was combined with antibiotics and tested against bacteria (Sara et al., 2021), whereas another study reported the synergistic effects of peptides-peptoids combinations against Gram-negative bacteria (Chongsiriwatana et al., 2011).

The interactions of peptide mimics RK610, RK758, and their combinations with model lipid membranes were systematically investigated using tBLM, QCM-D, and LB techniques, contributing to a better understanding of peptide mimic-lipid membrane interactions. In addition to studying the individual and combined effects of these mimics, the experimental scope was expanded to include their behaviour in the presence of the anionic lipid phosphatidylserine, POPS alongside DOPC

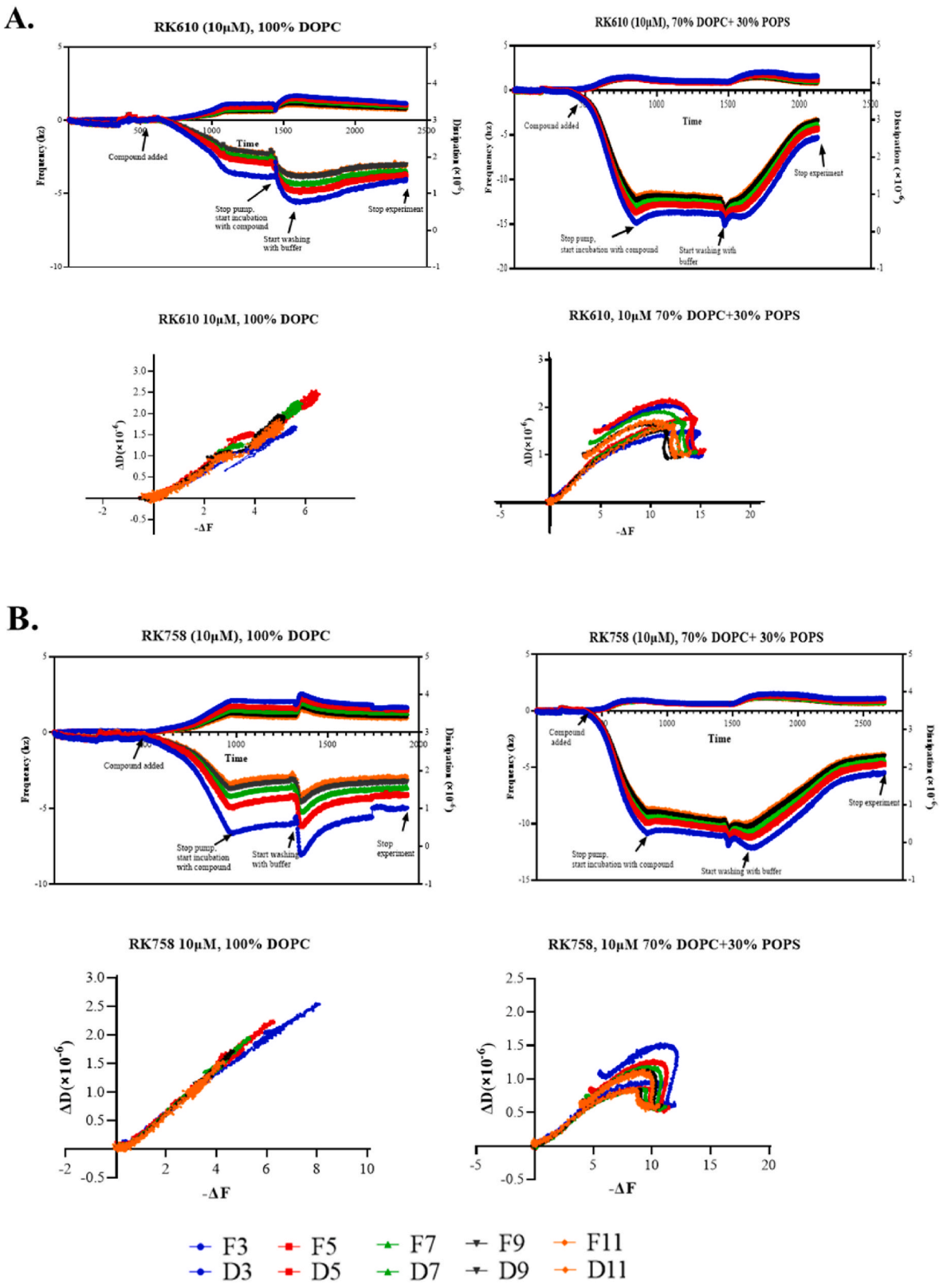

Fig. 6. QCM-D analysis of peptide mimics RK610 and RK758 on DOPC and DOPC + POPS lipid membranes. A. Effect of RK610 on DOPC and DOPC + POPS lipid membranes and the corresponding ΔF vs. ΔD plots highlighting the proportional (linear) and non-proportional (non-linear) effects on mass and rigidity for DOPC and DOPC + POPS, respectively. B. Effect of RK758 on DOPC and DOPC + POPS lipid membranes and the corresponding ΔF vs. ΔD plots, showing the relationship between mass adsorption and rigidity changes. The linear relationship for DOPC and non-linear relationship for DOPC + POPS indicated differences in interaction mechanisms.

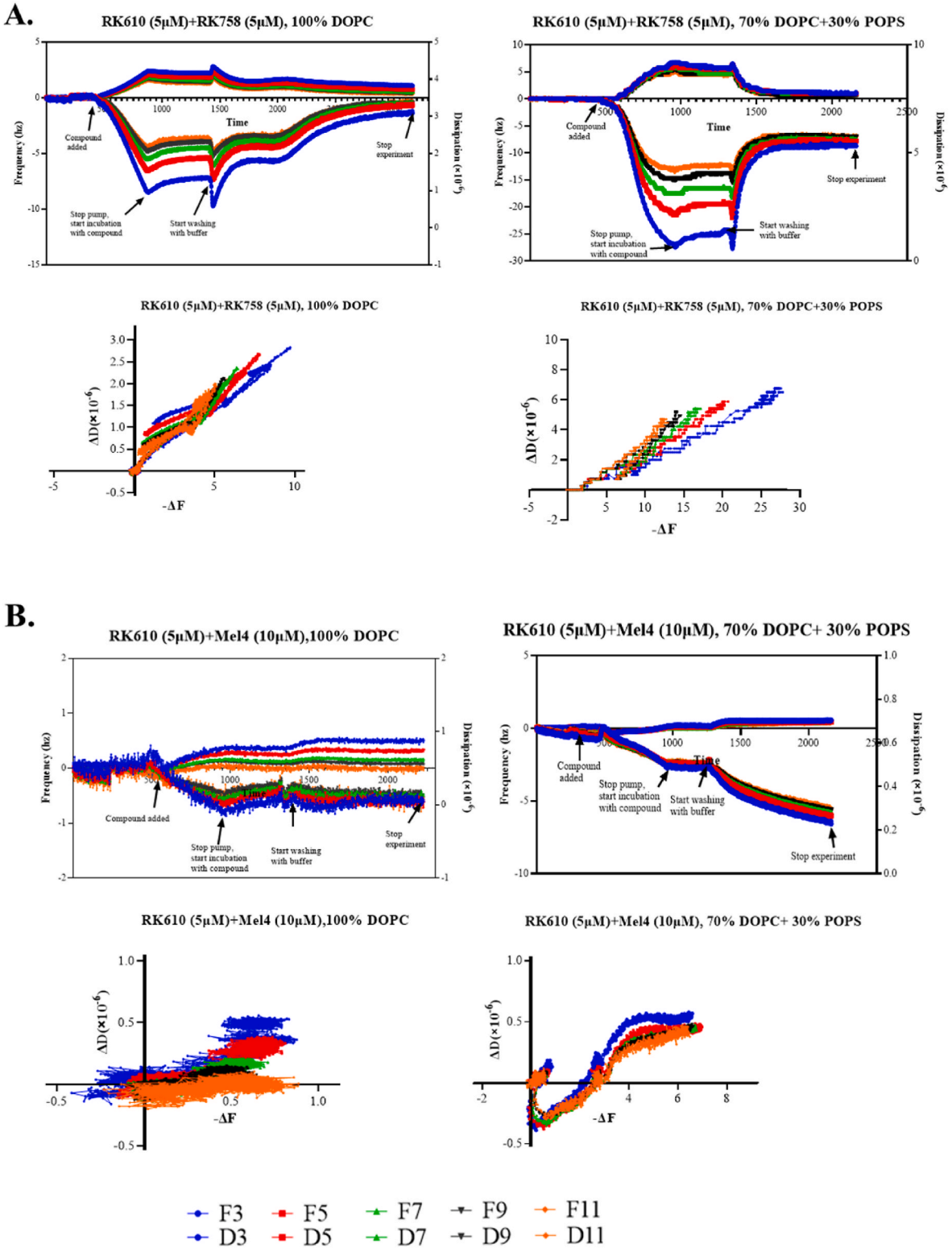

Fig. 7. QCM-D analysis of RK610+RK758 and RK610+Mel4 on DOPC and DOPC + POPS lipid membranes. A. Effect of RK610+RK758 on DOPC and DOPC + POPS lipid membranes and the corresponding ΔF vs. ΔD plots highlighting the proportional (linear) and non-proportional (non-linear) effects on mass and rigidity for DOPC and DOPC + POPS, respectively. B. Effect of RK610+Mel4 on DOPC and DOPC + POPS lipid membranes and the corresponding ΔF vs. ΔD plots, showing the relationship between mass adsorption and rigidity changes.

as previous reports highlighted the antiviral activity of membrane/envelope-targeting peptides and their mimics were heavily influenced by the composition of lipids (Teixeira et al., 2012; Vitiello et al., 2011). Extensive research has been conducted to elucidate the interactions between peptides and various lipids. Phosphatidylserine (PS) is a key lipid predominantly found in the inner leaflet of the mammalian plasma membrane, which becomes exposed on the surface of apoptotic or infected cells (Morizono and Chen, 2014). Viral envelopes often acquire

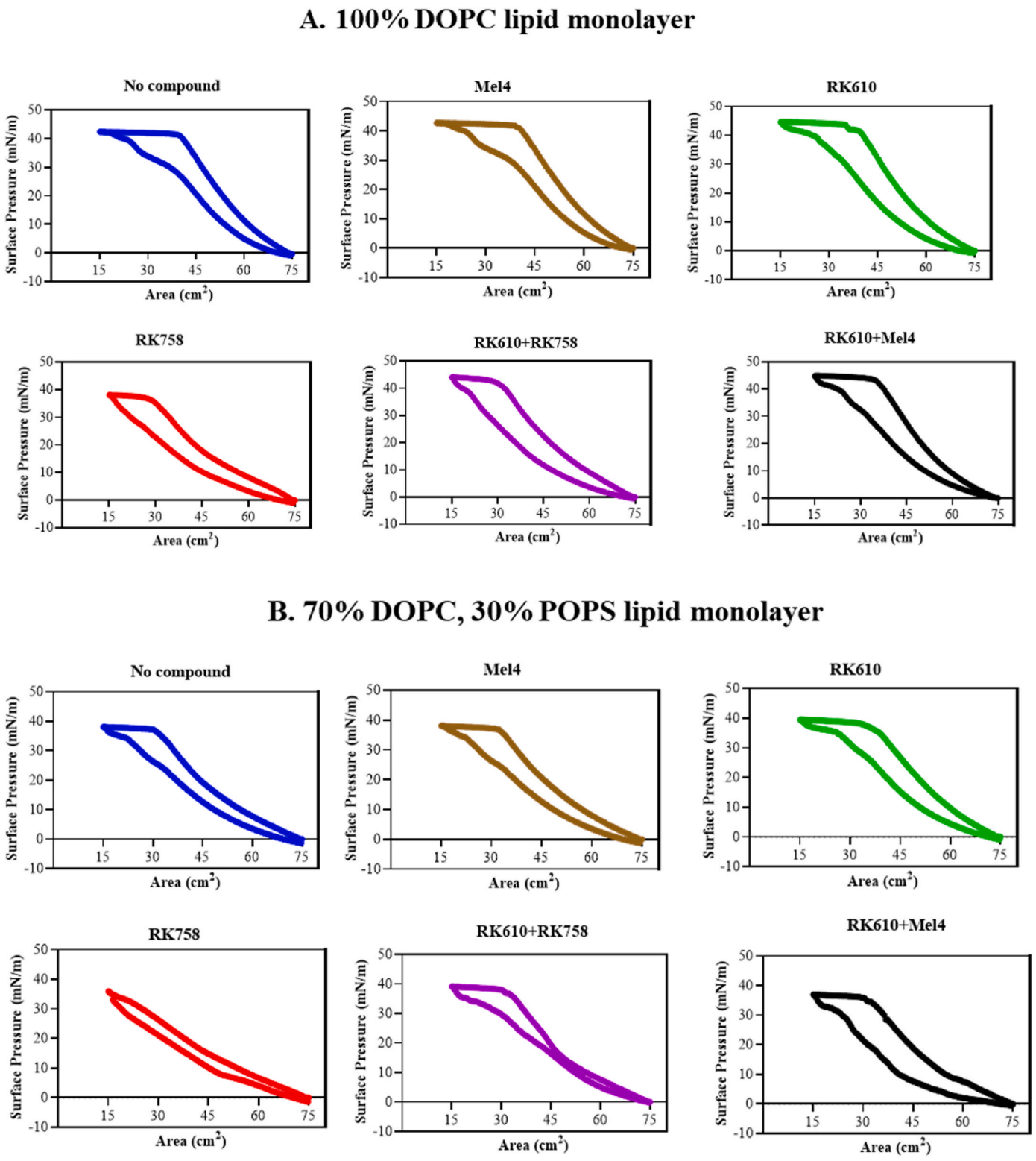

Fig. 8. Langmuir isotherms of peptide mimics and their combinations on DOPC (A) and DOPC + POPS (B) monolayers.

their lipid composition during budding from PS-enriched domains of the plasma membrane or the endoplasmic reticulum (Fraser, 2019), making PS a critical component of the viral lipid envelope. By targeting PS-enriched membranes, peptide mimics could selectively target viral envelopes while sparing host membranes lacking PS exposure (Saud et al., 2022; Van Meer et al., 2008). Understanding how peptide mimics interact with PS-enriched membranes could enhance the knowledge of their mechanisms of viral particle interaction and the influence of membrane composition on their activity. To explore the interactions of peptide mimics RK610 and RK758 with model lipid membranes, two distinct lipid compositions (100 % DOPC and 70 % DOPC + 30 % POPS) were employed. This approach was designed to examine how membrane composition influences the behaviour of peptide mimics. DOPC, a zwitterionic phospholipid, represents a neutral bilayer that mimics the

outer leaflet of eukaryotic cell membranes (Lütgebaucks et al., 2017; Smolentsev et al., 2016). In contrast, the inclusion of POPS, an anionic phospholipid, introduces a negative charge, simulating the inner leaflet of mammalian cell membranes, microbial membranes rich in acidic phospholipids, or mammalian cell membranes following viral infection (Kawabata et al., 2023; Lütgebaucks et al., 2017; Smolentsev et al., 2016). By comparing the interactions of the peptide mimics—both individually and in combination—with these two lipid bilayers, the role of lipid composition in the mimics' activity was evaluated. In tBLM studies, the individual effects of the peptide mimics did not differentiate between the two lipid compositions in terms of conductance. However, when tested in combination, the peptides and mimics significantly reduced conductance in both bilayers, indicating enhanced membrane-binding properties compared to their individual effects. In contrast, Mel4 showed no attachment to either lipid membrane. These findings for Mel4 were consistent with earlier reports indicating no significant interactions (Berry et al., 2018). Other studies had also explored the impact of peptides and their mimics on a range of lipids, including cholesterol, phosphatidylcholine, phosphatidylserine, diphytanyl-diglyceride ether, and phosphatidylglycerol (Alvares et al., 2017; Bahatheg et al., 2024; Mohid et al., 2022). While this specific class of peptide mimics had not been previously studied against lipid bilayers using tBLM (Berry et al., 2018), other peptide mimics, such as cholic acid-based, biphenyl-based amphiphilic cationic, N-naphthoyl-phenylglyoxamide-based, biphenylglyoxamide-based, and N-sulfonylphenyl-glyoxamide-based compounds, had been reported to exhibit contrasting behaviour, increasing conductance in lipid bilayers (Kuppusamy et al., 2018; Nizalapur et al., 2016; Wu et al., 2022). In contrast, anthranilamide-based peptide mimics like RK610 and RK758 reduced conductance, whether tested alone or in combination. This suggests that the insertion of these molecules into lipid bilayers alters the lipid packing such that spontaneous membrane pores are less likely to be formed (Alghalayini et al., 2019).

The QCM-D and LB experiments provided complementary ideas into the interactions of peptide mimics with lipid membranes, particularly regarding their impact on membrane stability, rigidity, and packing. While QCM-D measured the dynamic mass adsorption and viscoelastic changes upon peptide-lipid interaction, the LB isotherms captured how these interactions influenced monolayer stability and lipid packing at controlled surface pressures. In DOPC membranes, QCM-D revealed that RK610 and RK758 caused significant mass adsorption with a slight decrease in rigidity, as indicated by a linear ΔF *vs.* ΔD relationship. This proportionality suggested direct membrane binding behaviour, which was also observed in previous studies on wild-type uperin 3.5 interacting with mammalian membranes (John et al., 2018). However, alternative interpretations exist, as similar linear patterns in Gly15Gly19-caerin 1.1 interactions were attributed to peptide aggregation on the membrane surface (McCubbin et al., 2011). The LB results further supported this, showing that RK610 increased the surface pressure, indicating tighter lipid packing, while RK758 reduced the pressure, suggesting a disruptive effect on lipid organization. The RK610+RK758 combination in both QCM-D and LB experiments exhibited stronger interactions than either mimic alone, with increased mass adsorption (QCM-D) and higher surface pressure with reduced plateau area (LB). For Mel4, QCM-D showed negligible interaction with DOPC, aligning with LB data where Mel4 alone did not significantly alter surface pressure or plateau area. However, when combined with RK610, QCM-D detected weak binding and partial membrane insertion, which was also reflected in the LB data as a slight increase in surface pressure but no major changes in the plateau area. This suggests that Mel4 might slightly influence membrane behaviour in the presence of other peptide mimics, but did not strongly interact with lipid monolayers alone.

The addition of POPS to the lipid composition significantly enhanced peptide-lipid interactions, as observed in both techniques. In QCM-D, RK610 and RK758 exhibited greater frequency shifts and more pronounced changes in dissipation, suggesting stronger membrane interactions. Correspondingly, in LB experiments, RK758 caused a notable reduction in surface pressure and eliminated the plateau region, indicating a destabilizing effect, whereas RK610 increased the plateau area, suggesting enhanced monolayer flexibility. The RK610+RK758 combination in POPS-containing membranes showed strong mass adsorption in QCM-D and increased surface pressure in LB, but with a linear ΔF *vs.* ΔD relationship, indicating a proportional mass-rigidity interaction. Interestingly, the RK610+Mel4 combination in POPS-containing membranes exhibited moderate interactions in both techniques. QCM-D showed non-linear mass-rigidity relationships, indicating complex interaction dynamics, while LB experiments detected a slight reduction in surface pressure without significant changes in the plateau area.

Many studies have reported that peptides and other compounds interacting with lipid membranes typically induce a negative frequency shift in QCM-D, accompanied by changes in rigidity. However, the ΔF *vs.* ΔD plots often exhibited distinct patterns, suggesting variations in the mode of action depending on the peptide and membrane composition (John et al., 2017, 2018; McCubbin et al., 2011; Wang et al., 2014). These differences highlighted the diverse mechanistic pathways through which peptides or mimics could interact with lipid membranes, ranging from surface adsorption and aggregation to insertion and disruption (John et al., 2018). Similarly, Langmuir-Blodgett experiments had been extensively used to investigate the behaviour of peptides on lipid monolayers, providing complementary observations into peptide-membrane interactions.

Previous studies on antimicrobial peptides had demonstrated that their effects on lipid monolayers vary depending on both peptide and lipid type. For instance, RK758 caused a decrease in surface pressure, a behaviour also observed for LL-37 (Pastuszak et al., 2023) and 7S globulin peptides (Zou et al., 2018). In contrast, RK610 and its combinations exhibited behaviours similar to those of protegrin-1 (Ishitsuka et al., 2006), androctonin (Hetru et al., 2000), δ-lysin (Bhakoo et al., 1982), and melittin (Maget-Dana, 1999), which increased surface pressure by stabilizing lipid packing. The lipid composition also played a significant role in modulating the interaction of peptide mimics with lipid monolayers, where they behaved differently against zwitterionic lipid DOPC and in the presence of anionic lipids like POPS. A comparable effect was reported for melittin, which exhibited higher affinity for phosphatidylglycerol monolayers compared to choline-containing monolayers in Langmuir experiments (Hendrickson et al., 1983).

The synergistic and additive effects observed in this study further highlight the therapeutic potential of peptide mimics combinations. These combinations achieved enhanced antiviral activity at lower concentrations, reducing the likelihood of cytotoxicity and off-target effects. Mechanistic findings from tBLM, QCM-D, Langmuir, and complementary techniques such as TEM emphasized the lipid-targeting nature of these peptide mimics, which was a key to their antiviral efficacy. Future research should investigate the structural and physicochemical properties that drive the observed synergy, with the aim of optimizing peptide mimic designs for improved specificity, potency, and reduced toxicity. Evaluating *in vivo* safety efficacy, pharmacokinetics, and stability of these combinations will also be critical for advancing their clinical potential. Furthermore, incorporating TEM studies of lipid vesicles to directly visualize vesicle disruption or modification by these agents may complement the current methods and provide more mechanistic insights. In summary, this research establishes a strong foundation for developing peptide mimic-based antiviral strategies. By exploring the synergistic effects and PS-mediated interactions observed in this study, these compounds could pave the way for broad-spectrum, envelope-targeting antiviral therapies with minimal toxicity and enhanced efficacy.

5. Conclusions

This study highlights the promising potential of peptide mimics

RK610 and RK758, both individually and in combination. Specifically, the combination of RK610+RK758 showed strong antiviral effects against MHV-1 and H1N1, while RK610+Mel4 was particularly effective against HSV-1, achieving notable results at lower concentrations while maintaining cellular safety. Further tests with lipid layers highlighted the significant impact of these combinations on viral membranes, with RK610+RK758 showing the most pronounced effect, and TEM imaging confirmed structural damage to viral particles, further supporting the efficacy of these combinations. Besides this, biophysical techniques revealed that the interaction of these peptide mimics with lipid layers was influenced by individual and combination of compounds and membrane lipid composition, with the presence of negatively charged phosphatidylserine enhancing these interactions. This research offers valuable observations into developing broad-spectrum antiviral therapies that target the unique lipid structures of viral envelopes, particularly those enriched with PS. It provides a promising strategy to combat viruses while minimizing side effects and reducing the risk of resistance development.

CRediT authorship contribution statement

Umme Laila Urmi: Writing – original draft, Methodology, Investigation, Formal analysis, Conceptualization. **Ajay Kumar Vijay:** Writing – review & editing, Supervision, Resources, Methodology, Conceptualization. **Rajesh Kuppusamy:** Writing – review & editing, Resources, Methodology, Conceptualization. **Samuel Attard:** Writing – review & editing, Resources, Formal analysis. **Lissy M. Hartmann:** Writing – review & editing, Methodology, Formal analysis. **Samara Bridge:** Writing – review & editing, Methodology, Formal analysis. **Suganeya Soundararajan:** Writing – review & editing, Methodology, Formal analysis. **Stephen A. Holt:** Methodology, Investigation, Formal analysis. **Sidra Sarwat:** Writing – review & editing, Methodology, Formal analysis. **Salequl Islam:** Writing – review & editing, Supervision, Conceptualization. **Charles G. Cranfield:** Writing – review & editing, Supervision, Resources, Formal analysis. **Naresh Kumar:** Writing – review & editing, Supervision, Resources. **Mark D.P. Willcox:** Writing – review & editing, Supervision, Resources, Methodology, Conceptualization.

Funding

This research did not receive any specific grant from funding agencies in the public, commercial, or not-for-profit sectors.

Declaration of competing interest

The authors declare that they have no known competing financial interests or personal relationships that could have appeared to influence the work reported in this paper.

Appendix A. Supplementary data

Supplementary data to this article can be found online at https://doi.org/10.1016/j.virol.2025.110599.

Data availability

Data will be made available on request.

References

Aldilla, V.R., Chen, R., Kuppusamy, R., Chakraborty, S., Willcox, M.D., Black, D.S., Thordarson, P., Martin, A.D., Kumar, N., 2022. Hydrogels with intrinsic antibacterial activity prepared from naphthyl anthranilamide (NaA) capped peptide mimics. Sci. Rep. 12 (1), 22259.

Alghalayini, A., Garcia, A., Berry, T., Cranfield, C.G., 2019. The use of tethered bilayer lipid membranes to identify the mechanisms of antimicrobial peptide interactions with lipid bilayers. Antibiotics 8 (1), 12.

Alvares, D.S., Neto, J.R., Ambroggio, E.E., 2017. Phosphatidylserine lipids and membrane order precisely regulate the activity of Polybia-MP1 peptide. Biochimica et Biophysica Acta (BBA)-Biomembranes 1859 (6), 1067–1074.

Amblard, F., Zhou, S., Liu, P., Yoon, J., Cox, B., Muzzarelli, K., Kuiper, B.D., Kovari, L.C., Schinazi, R.F., 2018. Synthesis and antiviral evaluation of novel peptidomimetics as norovirus protease inhibitors. Bioorg. Med. Chem. Lett 28 (12), 2165–2170.

Bahatheg, G., Kuppusamy, R., Yasir, M., Bridge, S., Mishra, S.K., Cranfield, C.G., Black, D. S., Willcox, M., Kumar, N., 2024. Dimeric peptoids as antibacterial agents. Bioorg. Chem. 147, 107334.

Bai, L., Xu, J., Zeng, L., Zhang, L., Zhou, F., 2024. A review of HSV pathogenesis, vaccine development, and advanced applications. Molecular Biomedicine 5 (1), 35.

Belardo, G., Cenciarelli, O., La Frazia, S., Rossignol, J.F., Santoro, M.G., 2015. Synergistic effect of nitazoxanide with neuraminidase inhibitors against influenza A viruses in vitro. Antimicrob. Agents Chemother. 59 (2), 1061–1069.

Berry, T., Dutta, D., Chen, R., Leong, A., Wang, H., Donald, W.A., Parviz, M., Cornell, B., Willcox, M., Kumar, N., 2018. Lipid membrane interactions of the cationic antimicrobial peptide chimeras melimine and cys-melimine. Langmuir 34 (38), 11586–11592.

Bhakoo, M., Birkbeck, T.H., Freer, J.H., 1982. Interaction of Staphylococcus aureus. delta.-lysin with phospholipid monolayers. Biochemistry 21 (26), 6879–6883.

Chongsiriwatana, N.P., Wetzler, M., Barron, A.E., 2011. Functional synergy between antimicrobial peptoids and peptides against Gram-negative bacteria. Antimicrob. Agents Chemother. 55 (11), 5399–5402.

Chou, S., Ercolani, R.J., Derakhchan, K., 2018. Antiviral activity of maribavir in combination with other drugs active against human cytomegalovirus. Antivir. Res. 157, 128–133.

Criscuolo, E., Clementi, N., Mancini, N., Burioni, R., Miduri, M., Castelli, M., Clementi, M., 2018. Synergy evaluation of anti-Herpes Simplex Virus type 1 and 2 compounds acting on different steps of virus life cycle. Antivir. Res. 151, 71–77.

Dahal, A., Sonju, J.J., Kousoulas, K.G., Jois, S.D., 2022. Peptides and peptidomimetics as therapeutic agents for Covid-19. Peptide Science 114 (1), e24245.

Dai, W., Jochmans, D., Xie, H., Yang, H., Li, J., Su, H., Chang, D., Wang, J., Peng, J., Zhu, L., 2021. Design, synthesis, and biological evaluation of peptidomimetic aldehydes as broad-spectrum inhibitors against enterovirus and SARS-CoV-2. J. Med. Chem. 65 (4), 2794–2808.

Drajkowska, A., Molski, A., 2025. Transmembrane clustering of short amyloid peptide fragments: a coarse grained molecular dynamics study. Biophys. Chem. 320, 107418.

Dutta, D., Zhao, T., Cheah, K.B., Holmlund, L., Willcox, M.D., 2017. Activity of a melimine derived peptide Mel4 against Stenotrophomonas, Delftia, Elizabethkingia, Burkholderia and biocompatibility as a contact lens coating. Contact Lens Anterior Eye 40 (3), 175–183.

Fraser, M.E., 2019. Novel Anti-viral Strategies for Lipid-Enveloped Viruses. University of Notre Dame.

Grassin, E. Cooperative Interaction of Antimicrobial Peptides as an Emerging Novel Mechanism of Host Defense.

Hartmann, L.M., Garcia, A., Deplazes, E., Cranfield, C.G., 2022. Determining the pore size of multimeric peptide ion channels using cation conductance measures of tethered bilayer lipid membranes. Membrane Lipids: Methods Protoc. 81–92.

Hendrickson, H.S., Fan, P.C., Kaufman, D.K., Kleiner, D.E., 1983. The effect of a phase transition on penetration of phospholipid monolayers by melittin and glucagon. Arch. Biochem. Biophys. 227 (1), 242–247.

Herring, S., Oda, J.M., Wagoner, J., Kirchmeier, D., O'Connor, A., Nelson, E.A., Huang, Q., Liang, Y., DeWald, L.E., Johansen, L.M., 2021. Inhibition of arenaviruses by combinations of orally available approved drugs. Antimicrob. Agents Chemother. 65 (4). https://doi.org/10.1128/aac.01146-01120.

Hetru, C., Letellier, L., Oren, Z., Hoffmann, J.A., Shai, Y., 2000. Androctonin, a hydrophilic disulphide-bridged non-haemolytic anti-microbial peptide: a plausible mode of action. Biochem. J. 345 (3), 653–664.

Ianevski, A., Zusinaite, E., Tenson, T., Oksenych, V., Wang, W., Afset, J.E., Bjørås, M., Kainov, D.E., 2022. Novel synergistic anti-enteroviral drug combinations. Viruses 14 (9), 1866.

Ishitsuka, Y., Pham, D.S., Waring, A.J., Lehrer, R.I., Lee, K.Y.C., 2006. Insertion selectivity of antimicrobial peptide protegrin-1 into lipid monolayers: effect of head group electrostatics and tail group packing. Biochimica et Biophysica Acta (BBA)-Biomembranes 1758 (9), 1450–1460.

Jeffreys, L.N., Pennington, S.H., Duggan, J., Caygill, C.H., Lopeman, R.C., Breen, A.F., Jinks, J.B., Ardrey, A., Donnellan, S., Patterson, E.I., 2022. Remdesivir–ivermectin combination displays synergistic interaction with improved in vitro activity against SARS-CoV-2. Int. J. Antimicrob. Agents 59 (3), 106542.

John, T., Abel, B., Martin, L.L., 2018. The quartz crystal microbalance with dissipation monitoring (QCM-D) technique applied to the study of membrane-active peptides. Aust. J. Chem. 71 (7), 543–546.

John, T., Voo, Z.X., Kubeil, C., Abel, B., Graham, B., Spiccia, L., Martin, L.L., 2017. Effects of guanidino modified aminoglycosides on mammalian membranes studied using a quartz crystal microbalance. MedChemComm 8 (5), 1112–1120.

Kawabata, K., Sato, Y., Kubo, T., Tokumura, A., Nishi, H., Morimoto, K., 2023. Phospholipid analysis of two influenza A virus-infected cell lines differing in their viral replication kinetics. Arch. Virol. 168 (5), 132. https://doi.org/10.1007/s00705-023-05766-x.

Kim, J.H., Grzincic, E.M., Yun, L., Spencer, R.K., Kline, M.A., Zuckermann, R.N., 2020. Lipid-anchor display on peptoid nanosheets via co-assembly for multivalent pathogen recognition. Soft Matter 16 (4), 907–913.

Kruse, H.V., Chakraborty, S., Chen, R., Kumar, N., Yasir, M., Lewin, W.T., Suchowerska, N., Willcox, M.D., McKenzie, D.R., 2024. Protecting orthopaedic implants from infection: antimicrobial peptide Mel4 is non-toxic to bone cells and

reduces bacterial colonisation when bound to plasma ion-implanted 3D-printed PAEK polymers. Cells 13 (8), 656.
Kuppusamy, R., Yasir, M., Berry, T., Cranfield, C.G., Nizalapur, S., Yee, E., Kimyon, O., Taunk, A., Ho, K.K., Cornell, B., 2018. Design and synthesis of short amphiphilic cationic peptidomimetics based on biphenyl backbone as antibacterial agents. Eur. J. Med. Chem. 143, 1702–1722.
Kuppusamy, R., Yasir, M., Yu, T.T., Voli, F., Vittorio, O., Miller, M.J., Lewis, P., Black, D. S., Willcox, M., Kumar, N., 2023. Tuning the anthranilamide peptidomimetic design to selectively target planktonic bacteria and biofilm. Antibiotics 12 (3), 585.
Liuzzi, M., Déziel, R., Moss, N., Beaulieu, P., Bonneau, A.-M., Bousquet, C., Chafouleas, J. G., Garneau, M., Jaramillo, J., Krogsrud, R.L., 1994. A potent peptidomimetic inhibitor of HSV ribonucleotide reductase with antiviral activity in vivo. Nature 372 (6507), 695–698.
Luganini, A., Nicoletto, S.F., Pizzuto, L., Pirri, G., Giuliani, A., Landolfo, S., Gribaudo, G., 2011. Inhibition of herpes simplex virus type 1 and type 2 infections by peptide-derivatized dendrimers. Antimicrob. Agents Chemother. 55 (7), 3231–3239.
Lütgebaucks, C., Macias-Romero, C., Roke, S., 2017. Characterization of the interface of binary mixed DOPC: DOPS liposomes in water: the impact of charge condensation. J. Chem. Phys. 146 (4).
Maget-Dana, R., 1999. The monolayer technique: a potent tool for studying the interfacial properties of antimicrobial and membrane-lytic peptides and their interactions with lipid membranes. Biochimica et Biophysica Acta (BBA)-Biomembranes 1462 (1–2), 109–140.
McCubbin, G.A., Praporski, S., Piantavigna, S., Knappe, D., Hoffmann, R., Bowie, J.H., Separovic, F., Martin, L.L., 2011. QCM-D fingerprinting of membrane-active peptides. Eur. Biophys. J. 40, 437–446.
Mechler, A., Praporski, S., Atmuri, K., Boland, M., Separovic, F., Martin, L.L., 2007. Specific and selective peptide-membrane interactions revealed using quartz crystal microbalance. Biophys. J. 93 (11), 3907–3916.
Mohid, S.A., Sharma, P., Alghalayini, A., Saini, T., Datta, D., Willcox, M.D., Ali, H., Raha, S., Singha, A., Lee, D., 2022. A rationally designed synthetic antimicrobial peptide against Pseudomonas-associated corneal keratitis: structure-function correlation. Biophys. Chem. 286, 106802.
Morizono, K., Chen, I.S., 2014. Role of phosphatidylserine receptors in enveloped virus infection. J. Virol. 88 (8), 4275–4290.
Neffe, A.T., Meyer, B., 2004. A peptidomimetic HIV-entry inhibitor directed against the CD4 binding site of the viral glycoprotein gp120. Angew. Chem. Int. Ed. 43 (22), 2937–2940.
Nikolaeva-Glomb, L., Galabov, A.S., 2004. Synergistic drug combinations against the in vitro replication of Coxsackie B1 virus. Antivir. Res. 62 (1), 9–19.
Nizalapur, S., Ho, K.K., Kimyon, Ö., Yee, E., Berry, T., Manefield, M., Cranfield, C.G., Willcox, M., Black, D.S., Kumar, N., 2016. Synthesis and biological evaluation of N-naphthoyl-phenylglyoxamide-based small molecular antimicrobial peptide mimics as novel antimicrobial agents and biofilm inhibitors. Org. Biomol. Chem. 14 (14), 3623–3637.
Ó Gráda, C., 2024. H1N1 and WW1: the Spanish Flu and the Great War.
Organization, W.H., 2024. Number of COVID-19 Deaths Reported to WHO (Cumulative Total). WHO. Retrieved 10 May 2024 from. https://data.who.int/dashboards/covid19/deaths.
Pastuszak, K., Kowalczyk, B., Tarasiuk, J., Luchowski, R., Gruszecki, W.I., Jurak, M., Palusinska-Szysz, M., 2023. Insight into the mechanism of interactions between the LL-37 peptide and model membranes of Legionella gormanii bacteria. Int. J. Mol. Sci. 24 (15), 12039.
Perez-Lopez, S., Vila-Romeu, N., Alsina Esteller, M.A., Espina, M., Haro, I., Mestres, C., 2009. Interaction of GB virus C/hepatitis G virus synthetic peptides with lipid Langmuir monolayers and large unilamellar vesicles. J. Phys. Chem. B 113 (1), 319–327.
R Dennison, S., Harris, F., A Phoenix, D., 2010. A Langmuir approach using monolayer interactions to investigate surface active peptides. Protein Pept. Lett. 17 (11), 1363–1375.
Rasul, R., Cole, N., Balasubramanian, D., Chen, R., Kumar, N., Willcox, M., 2010. Interaction of the antimicrobial peptide melimine with bacterial membranes. Int. J. Antimicrob. Agents 35 (6), 566–572.
Sara, M., Kuppusamy, R., Afzal, M., Khan, M., Yasir, M., Kalaiselvan, P., Hui, A., Kumar, N., Willcox, M.D., 2021. Synergistic activity of a peptide mimic with quinolones and cephalosporins against Staphylococcus aureus. Investig. Ophthalmol. Vis. Sci. 62 (8), 400-400.
Saud, Z., Tyrrell, V.J., Zaragkoulias, A., Protty, M.B., Statkute, E., Rubina, A., Bentley, K., White, D.A., Rodrigues, P.D.S., Murphy, R.C., Köfeler, H., Griffiths, W.J., Alvarez-Jarreta, J., Brown, R.W., Newcombe, R.G., Heyman, J., Pritchard, M., McLeod, R.W., Arya, A., Stanton, R.J., 2022. The SARS-CoV2 envelope differs from host cells, exposes procoagulant lipids, and is disrupted in vivo by oral rinses. J. Lipid Res. 63 (6), 100208. https://doi.org/10.1016/j.jlr.2022.100208.
Scala, M.C., Marchetti, M., Superti, F., Agamennone, M., Campiglia, P., Sala, M., 2023. Rational design of novel peptidomimetics against influenza A virus: biological and computational studies. Int. J. Mol. Sci. 24 (18), 14268.
Shyr, Z.A., Cheng, Y.-S., Lo, D.C., Zheng, W., 2021. Drug combination therapy for emerging viral diseases. Drug Discov. Today 26 (10), 2367–2376.
Smolentsev, N., Lütgebaucks, C., Okur, H.I., De Beer, A.G., Roke, S., 2016. Intermolecular headgroup interaction and hydration as driving forces for lipid transmembrane asymmetry. J. Am. Chem. Soc. 138 (12), 4053–4060.
Souza, P.F., 2022. Synthetic antimicrobial peptides for controlling fungi in foods. Curr. Opin. Food Sci. 45, 100819.
Strandberg, E., Zerweck, J., Horn, D., Pritz, G., Berditsch, M., Bürck, J., Wadhwani, P., Ulrich, A.S., 2015. Influence of hydrophobic residues on the activity of the antimicrobial peptide magainin 2 and its synergy with PGLa. J. Pept. Sci. 21 (5), 436–445.
Sun, W., He, S., Martínez-Romero, C., Kouznetsova, J., Tawa, G., Xu, M., Shinn, P., Fisher, E.G., Long, Y., Motabar, O., 2017. Synergistic drug combination effectively blocks Ebola virus infection. Antivir. Res. 137, 165–172.
Teixeira, V., Feio, M.J., Bastos, M., 2012. Role of lipids in the interaction of antimicrobial peptides with membranes. Prog. Lipid Res. 51 (2), 149–177.
Urmi, U.L., Attard, S., Vijay, A.K., Willcox, M.D., Kumar, N., Islam, S., Kuppusamy, R., 2023. Antiviral activity of anthranilamide peptidomimetics against Herpes simplex virus 1 and a coronavirus. Antibiotics 12 (9), 1436.
Urmi, U.L., Vijay, A.K., Willcox, M.D., Attard, S., Enninful, G., Kumar, N., Islam, S., Kuppusamy, R., 2024. Exploring the efficacy of peptides and mimics against influenza A virus, adenovirus, and murine norovirus. Int. J. Mol. Sci. 25 (13), 7030.
Van Meer, G., Voelker, D.R., Feigenson, G.W., 2008. Membrane lipids: where they are and how they behave. Nat. Rev. Mol. Cell Biol. 9 (2), 112–124.
Vitiello, G., Falanga, A., Galdiero, M., Marsh, D., Galdiero, S., D'Errico, G., 2011. Lipid composition modulates the interaction of peptides deriving from herpes simplex virus type I glycoproteins B and H with biomembranes. Biochimica et Biophysica Acta (BBA)-Biomembranes 1808 (10), 2517–2526.
Wang, K.F., Nagarajan, R., Camesano, T.A., 2014. Antimicrobial peptide alamethicin insertion into lipid bilayer: a QCM-D exploration. Colloids Surf., B Biointerfaces 116, 472–481.
Wang, K.F., Nagarajan, R., Camesano, T.A., 2015. Differentiating antimicrobial peptides interacting with lipid bilayer: molecular signatures derived from quartz crystal microbalance with dissipation monitoring. Biophys. Chem. 196, 53–67.
Wu, J., Yu, T.T., Kuppusamy, R., Hassan, M.M., Alghalayini, A., Cranfield, C.G., Willcox, M.D., Black, D.S., Kumar, N., 2022. Cholic acid-based antimicrobial peptide mimics as antibacterial agents. Int. J. Mol. Sci. 23 (9), 4623.
Zou, Y., Pan, R., Ruan, Q., Wan, Z., Guo, J., Yang, X., 2018. Interaction of soybean 7s globulin peptide with cell membrane model via isothermal titration calorimetry, quartz crystal microbalance with dissipation, and Langmuir monolayer study. J. Agric. Food Chem. 66 (19), 4913–4922.